Searching for long strings in CMB maps

L. Perivolaropoulos*
Department of Physics, University of Crete, P.O. Box 2208, 710 03 Heraklion, Crete, Greece
(Received 30 March 1998; published 8 October 1998)

Using analytical methods and Monte Carlo simulations, we analyze new statistics designed to detect isolated step-like discontinuities which are coherent over large areas of cosmic microwave background pixel maps. Such coherent temperature discontinuities are predicted by the *Kaiser-Stebbins* effect to form due to long cosmic strings in our present horizon. The background of the coherent step-like seed is assumed to be a scale invariant Gaussian random field which could have been produced by a superposition of seeds on smaller scales and/or by inflationary quantum fluctuations. We find that the proposed statistics can detect the presence of a coherent discontinuity at a sensitivity level almost an order of magnitude better compared to more conventional statistics such as skewness or kurtosis. [S0556-2821(98)11720-4]

PACS number(s): 98.80.Es

I. INTRODUCTION

The major progress achieved during the past 15 years in both theory and cosmological observations has turned the search for the origin of cosmic structure into one of the most exciting fields of scientific research. Despite the severe constraints imposed by detailed observational data on theories for structure formation, the central question remains open: *What is the origin of primordial fluctuations that gave rise to structure in the universe?* Two classes of theories attempting to answer this question have emerged during the past twenty years and have managed to survive through the observational constraints with only minor adjustments.

According to the first class, primordial fluctuations are produced by quantum fluctuations of a linearly coupled scalar field during a period of inflation [1]. These fluctuations are subsequently expected to become classical and provide the progenitors of structure in the universe. Because of the extremely small linear coupling of the scalar field, needed to preserve the observed large scale homogeneity, the inflationary perturbations are expected by the central limit theorem to obey Gaussian statistics. This is not the case for the second class of theories.

According to this second class [2], primordial perturbations are provided by *seeds* of trapped energy density produced during symmetry breaking phase transitions in the early universe. Such symmetry breaking is predicted by grand unified theories (GUTs) to occur at early times as the universe cools and expands. The geometry of the produced seeds, known as *topological defects* is determined by the topology of the vacuum manifold of the physically realized GUT. Thus the defects may be pointlike (monopoles), linelike (cosmic strings), planar (domain walls) or collapsing pointlike (textures).

The cosmic string theory [3] for structure formation is the oldest and (together with textures [4]) best studied theory of the topological defect class. By fixing its single free parameter $G\mu$ (μ is the *effective* mass per unit length of the wiggly string G is Newtons constant and we have used units with $c=1$) to a value consistent with microphysical requirements coming from GUTs ($G\mu \simeq 10^{-6}$), the theory is consistent with the noise in pulsar signal arrival times assuming that the noise is due to gravitational radiation emitted by the defect network [5]. It may account for large scale filaments and sheets [6] (this is also the case with a large class of Gaussian models), galaxy formation at epochs $z \sim 2-3$ [7] (which could account well for quasars) and galactic magnetic fields [8]. With appropriate bias, it can also provide large scale peculiar velocities [9] and is consistent with the amplitude, spectral index [10] and the statistics [11] of the cosmic microwave background (CMB) anisotropies measured by the Cosmic Background Explorer (COBE) Collaboration [12] on large angular scales.

Various statistical tests have been applied on the Differential Microwave Radiometer (DMR) maps by the COBE team and all of them have indicated that the CMB fluctuations are Gaussian on these scales [13]. More recent studies [14] however applying non-standard statistical tests on the 4-year DMR maps have revealed the presence of non-Gaussian features on these maps. It is therefore important to design and apply new statistical tests on the available CMB data in order to verify or falsify the above claims for non-Gaussianity and to derive the characteristics of the discovered non-Gaussian features. There have been several interesting statistical tests proposed recently which attempt to address this issue on CMB [15] and large scale structure [16] data.

In spite of its attractive features, the cosmic string theory for structure formation is faced with problems on smaller angular scales if normalized on the COBE data. In particular, it has been shown [17] that the consistency of CMB data with the galaxy distribution data requires an enormous bias factor. In addition, it has been shown [18] that vector modes generically dominate in the CMB fluctuations induced by cosmic strings. This manifests itself as a domination of the scale invariant part of the string spectrum down to $1^\circ-2^\circ$ scales leading to a subdominant broad Doppler peak. This is not consistent with CMB data [19] which indicate the presence of a pronounced Doppler peak on these scales.

*Email address: leandros@physics.uch.gr

The above mentioned problems have recently reduced the interest on cosmic string based models. However one should not underestimate the fact that there are still significant uncertainties on both the data and the studies indicating the above results. The situation is expected to clarify as the theoretical studies get more refined and also when several planned CMB experiments [20,19] of equally high quality, but on smaller angular scales provide a wealth of new information within the next few years.

The CMB observations provide a valuable direct probe for identifying signatures of cosmic strings. The main mechanism by which strings can produce CMB fluctuations on angular scales larger than 1–2 degrees has been well studied both analytically [21] and using numerical simulations [10] and is known as the *Kaiser-Stebbins effect* [22]. According to this effect, moving long strings present between the time of recombination t_{rec} and the present time t_0, produce step-like temperature discontinuities between photons that reach the observer through opposite sides of the string. These discontinuities are due to the peculiar nature of the spacetime around a long string which even though is *locally* flat, *globally* has the geometry of a cone with deficit angle $8\pi G\mu$. The magnitude of the discontinuity is proportional to the deficit angle, to the string velocity v_s and depends on the relative orientation between the unit vector along the string $\hat{s}$ and the unit photon wave-vector $\hat{k}$. It is given by [21]

$$\frac{\delta T}{T} = \pm 4\pi G\mu v_s \gamma_s \hat{k}\cdot(\hat{v}_s \times \hat{s}) \tag{1}$$

where γ_s is the relativistic Lorentz factor and the sign changes when the string is crossed. The angular scale over which this discontinuity persists is given by the radius of curvature of the string which according to simulations [23] is approximately equal to the horizon scale.

The connection between the above mentioned vector modes and the Kaiser-Stebbins effect is made through the scale invariant part of the CMB spectrum which may be seen either as an outcome of the vector modes [18] or as a result of the Kaiser-Stebbins effect induced by strings on all scales from t_{rec} to t_0 [24].

As Eq. (1) indicates, the amplitude of the string induced discontinuity drops like $\cos\theta$ as we move away from the string. Thus on a typical sky patch of about $100^\circ \times 100^\circ$ with a string passing through its center, the amplitude of the discontinuity will drop at the edge of the map to about one half of its maximum value achieved in the region of the string. For the purposes of the statistics considered here which are based on nonlocal properties of CMB maps (differences of large sector temperatures), the $\cos\theta$ profile of the string induced discontinuity may be replaced by a step function with effective amplitude $4\pi G\mu_{eff} v_s\gamma_s = q 4\pi G\mu v_s\gamma_s$ where $q \in [1/2,1]$. The precise value of q may be obtained by demanding that the statistics applied on a map with a discontinuity described by the exact $\cos\theta$ profile and on a map with a discontinuity described by the approximate step function profile give the same results. We will not attempt the precise determination of the parameter q in this study because our goal is to suggest new statistics that can sensitively detect the presence of string induced discontinuities. The precise value of $G\mu$ is expected to be larger by the factor $1/q$ compared to the value $G\mu_{eff}$ corresponding to the effective step function that can be revealed by the proposed statistics.

The growth of the horizon from t_{rec} to t_0 results in a superposition of a large number of step-like temperature seeds of all sizes starting from about 2° (the angular size of the horizon at t_{rec}) to about 180° (the present horizon scale). By the central limit theorem, this large number of superposed seeds results in a pattern of fluctuations that obeys approximately Gaussian statistics. Thus the probability distribution for the temperature of each pixel of a CMB map with resolution larger than about $1^\circ - 2^\circ$ is Gaussian to a good approximation [18,25]. It has therefore been considered to be impossible to distinguish structure formation models based on cosmic strings from corresponding models based on inflation, using CMB maps with resolution angle larger than $1^\circ - 2^\circ$. Theoretical studies have thus focused on identifying the statistical signatures of cosmic strings on angular scales less than 1° [11] where the number of superposed seeds is smaller and the non-Gaussian character of fluctuations is expected to be stronger.[1]

These efforts however have been faced with the complicated and model dependent physical processes occurring on small angular scales. Such effects include isolated foreground point sources (particularly for high resolution CMB maps), reionization physics, string properties on small scales (kinks, loops, etc.) which require detailed simulations of both the string network and the cosmic background, in order to be properly taken into account. Even though there are preliminary efforts for such detailed simulations [18], it has become clear that it will take some time before theory and experiments on angular scales less than a few arcmin reach accuracy levels leading to detectable non-Gaussian string signatures.

An alternative approach to the problem is instead of focusing on small scales where the number of superposed seeds is small, to focus on larger angular scales where despite the large number of superposed seeds there is also coherence of induced fluctuations on large angular scales. Examples of studies along these lines include Refs. [27,28]. Fluctuations on these scales may be viewed as a superposition of a Gaussian scale invariant background coming mainly from small scale seeds plus a small number of step-like discontinuities which are coherent and persist on angular scales of order 100°. These are produced by long strings present in our present horizon. *Our goal is to find a statistic specially designed to detect this large scale coherence and use it to find the minimum amplitude of a coherent discontinuity that*

[1]The non-Gaussian features for texture maps are stronger than those of cosmic strings mainly because of the generically smaller number of textures per horizon volume [26].

can be detected at the $m\sigma$ ($m>1$) level relative to a given scale invariant or noise dominated Gaussian background. Such a statistic is equally effective on *any* angular resolution scale and its effectiveness is only diminished as the number of pixels of the CMB map is reduced or the noise is increased. The statistical variable we focus on, in Secs. II and III is the sample mean difference (SMD) of temperatures between large neighboring sectors of a CMB map. These sectors are separated by a random straight line in two dimensional maps or by a random point in one dimensional maps. The union of the two sectors gives back the complete map. We show that the statistics of the SMD variable are much more sensitive in detecting the presence of a coherent step-like seed than conventional statistics like the skewness or the kurtosis [29–31].

We also discuss an alternative statistic, the maximum sample difference (MSD) that is more sensitive in certain cases, but less robust than the SMD. This statistic is based on finding the maximum from a large sample of temperature differences between large neighboring sectors of CMB maps. We show that for noise dominated data the MSD statistic is even more sensitive than the SMD statistic. However, this sensitivity gets rapidly reduced when significant correlations are introduced in the underlying Gaussian data. Thus the MSD statistic is more sensitive, but less robust compared to the SMD statistic.

The structure of this paper is the following: In the next section titled ''Sample Mean Difference,'' we study analytically the statistics of the SMD variable and show that its average value is a sensitive quantity in detecting the presence of a randomly placed step-function on top of a Gaussian map. We then compare with the sensitivity of the *skewness* and *kurtosis* statistics. We find that the sensitivity of the SMD statistic is significantly superior to that of skewness and kurtosis in detecting the step function. These analytical results are shown for the case of one-dimensional maps, but the extension to the case of two dimensional maps is straightforward.

In the third section titled ''Monte Carlo Simulations,'' we perform Monte Carlo simulations of Gaussian maps with and without step-like discontinuities in one and two dimensions. Applying the skewness, kurtosis and average of SMD statistics on these maps, we verify the analytical results of Sec. II and find the minimum step-function amplitude that is detectable by the average SMD statistic. In Sec. IV we show both analytically and numerically that the MSD statistic can be significantly more sensitive and accurate even compared to the SMD statistic when applied to noise dominated data.

Finally in Sec. V we conclude, summarize and discuss the prospect of applying the average of SMD statistic and the MSD statistic to presently available CMB maps including the COBE data. That analysis [32] will be presented separately.

II. SAMPLE MEAN DIFFERENCE

Consider a one dimensional array of n pixel variables x_n. Let these variables be initially distributed according to a standardized Gaussian probability distribution. Consider now a step-function of amplitude 2α superposed so that the discontinuity is between pixels i_0 and i_0+1 (Fig. 1). The new probability distribution for a random pixel variable x is

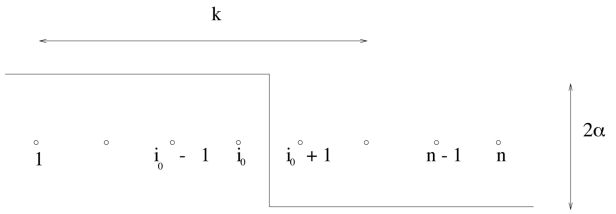

FIG. 1. A large scale coherent step-function discontinuity superposed on a one dimensional pixel map (the pixel-label k will be used in the definition of the SMD statistic and should not be confused with the kurtosis).

$$P(x)=\frac{f}{\sqrt{2\pi}}e^{-(x-\alpha)^2/2}+\frac{1-f}{\sqrt{2\pi}}e^{-(x+\alpha)^2/2} \tag{2}$$

where $f=i_0/n$. We are looking for a statistic that will optimally distinguish between a Gaussian array with a superposed step-function and a Gaussian array without one. The obvious statistics to try first are the moments of the distribution (2) with $\alpha=0$ and $\alpha\neq 0$.[2]

The moment generating function corresponding to Eq. (2) is

$$M(t)=fe^{\alpha t+t^2/2}+(1-f\ )e^{-\alpha t+t^2/2}. \tag{3}$$

It is straightforward to obtain all the distribution moments by differentiating the generating function [33] and using

$$\langle x_j^n\rangle=\left.\frac{d^nM}{dt^n}\right|_{t=0}. \tag{4}$$

The mean $\mu(\alpha,f\ )$, variance $\sigma^2(\alpha,f\ )$, skewness $s(\alpha,f\ )$ and kurtosis $k(\alpha,f\ )$ can be obtained in a straightforward way by proper differentiation of $M(t)$ as follows:

[2]With no loss of generality we may assume α positive or 0 because from the statistical point of view there is $\alpha\leftrightarrow-\alpha$ symmetry.

$$\mu(\alpha,f)\equiv\langle x\rangle=\alpha f-\alpha(1-f)$$

$$\sigma^2(\alpha,f)\equiv\langle(x-\mu)^2\rangle=1+4\alpha^2 f(1-f)$$

$$s(\alpha,f)\equiv\frac{\langle(x-\mu)^3\rangle}{\sigma^3}=\frac{8\alpha^3 f(1-3f+2f^2)}{(1+4\alpha^2 f(1-f))^{3/2}}$$

$$k(\alpha,f)\equiv\frac{\langle(x-\mu)^4\rangle}{\sigma^4}=\frac{3+8\alpha^2 f(3+2\alpha^2-3f^2-8\alpha^2 f+12\alpha^2 f^2-6\alpha^2 f^3)}{(1+4\alpha^2 f(1-f))^2}.$$

For $\alpha=0$ we obtain the Gaussian values for the skewness and the kurtosis $s(0,f)=0$, $k(0,f)=3$ as expected. For $\alpha\neq 0$ the moments deviate from the Gaussian values. In order to find the minimum value of α for which the moments can distinguish between a Gaussian pattern and a Gaussian+Step pattern, we must compare the deviation of moments from their Gaussian values with the standard deviation of the sample moments. The mean values of the skewness and the kurtosis are easily obtained by integrating with respect to f from 0 to 1, i.e., assuming that it is equally probable for the step-function to be superposed at any point of the lattice.

$$\overline{s}(\alpha)=\langle s(\alpha,f)\rangle=\int_0^1 df s(\alpha,f)=0 \tag{5}$$

$$\overline{k}(\alpha)=\langle k(\alpha,f)\rangle=\int_0^1 df k(\alpha,f). \tag{6}$$

These values are to be compared with the standard deviations of the moments, obtained as follows: The variance of the skewness over several n-pixel array realizations with fixed f and α is

$$\Delta s^2(\alpha,f)=\langle(\hat{s}-s)^2\rangle \tag{7}$$

where $\hat{s}\equiv s_1+\ldots+s_n/n$ is the sample skewness from a given pixel array realization, s is the actual skewness (for $n\to\infty$) and $s_i\equiv(x_i-\mu)^3/\sigma^3$ is the measured skewness on a given pixel. Now

$$\langle\hat{s}\rangle=\frac{n\langle s_1\rangle}{n}=\langle s_1\rangle=s. \tag{8}$$

Also

$$\langle\hat{s}^2\rangle=\frac{1}{n}\langle s_j^2\rangle+\left(1-\frac{1}{n}\right)\langle s_j\rangle^2 \tag{9}$$

where j is *any* pixel number ($j\in[1,n]$). Thus

$$\Delta s^2(\alpha,f)=\frac{1}{n}(\langle s_j^2\rangle-\langle s_j\rangle^2). \tag{10}$$

Similarly for the variance of the sample kurtosis, we have

$$\Delta k^2(\alpha,f)=\frac{1}{n}(\langle k_j^2\rangle-\langle k_j\rangle^2) \tag{11}$$

with $k_j=(1/\sigma^4)(x_j-\mu)^4$ and $\langle k_j^2\rangle=1/\sigma^8\langle(x_j-\mu)^8\rangle$.

The minimum value α_{min} of α detectable at 1σ level is obtained from the equations

$$\int_0^1 df[s(\alpha_{min},f)-\Delta s(\alpha_{min},f)]=0 \tag{12}$$

$$\int_0^1 df[(k(\alpha_{min},f)-3)-\Delta k(\alpha_{min},f)]=0. \tag{13}$$

Since [from Eq. (4)] $\overline{s}(\alpha)=0$ which is equal to the Gaussian value, the skewness can only be used to detect a step function by comparing the standard deviation $\Delta\overline{s}$ for $\alpha=0$ and $\alpha\neq 0$. By demanding $\Delta\overline{s}(\alpha_{min})\simeq 2\Delta\overline{s}(\alpha=0)$, we obtain $\alpha_{min}\simeq 2.5$. If instead we demand the standard deviation difference to be larger than 1σ, i.e., $\Delta\overline{s}(\alpha_{min})\simeq m\Delta\overline{s}(\alpha=0)$ with $m>2$, we obtain an even larger value for α_{min}. This result is independent of the number of pixels n. For the kurtosis we obtain from Eqs. (11), (13) $\alpha_{min}\simeq 4$ for $n=10^3$, while for $\alpha_{min}=0.5$, $n\simeq 10^6$ is required.

Using the alternative test, i.e., demanding $\Delta\overline{k}(\alpha_{min})\simeq 2\Delta\overline{k}(\alpha=0)$ we obtain $\alpha\simeq 2$ and this result is independent of the number of pixels n as in the case of skewness. Thus for the usual pixel maps where n is up to $O(1000)$, the kurtosis is not able to detect a step function with $|\alpha|\leqslant 2$ at the 1σ level.[3] This result remains unchanged for other statistical variables defined by *local* linear combinations of pixels (e.g., differences of neighboring pixel variables [11]) since the effect of a single discontinuity remains negligible if the long range coherence is not taken into account.

For CMB temperature maps with $(\delta T/T)_{rms}\simeq 2\times 10^{-5}$, the detectable value of $G\mu$ is

$$\alpha\equiv 4\pi G\mu(v_s\gamma_s)\cos\theta>2\left(\frac{\delta T}{T}\right)_{rms}\simeq 4\times 10^{-5}$$

$$\Rightarrow G\mu(v_s\gamma_s)\cos\theta\gtrsim 3\times 10^{-6} \tag{14}$$

[3]As in all cases discussed in this paper, α is measured in units of standard deviation (rms) of the underlying Gaussian map.

where θ is an angle obtained from the relative orientation of the string with respect to the observer. According to simulations $\langle v_s \gamma_s \rangle_{rms} \simeq 0.2$ and for $G\mu < 2\times 10^{-5}$, the detection of the Kaiser-Stebbins effect using statistics based on skewness and kurtosis is not possible. This excluded range however includes all the cosmologically interesting values of $G\mu$.

It is therefore important to look for alternative statistical variables that are more sensitive in detecting the presence of coherent discontinuities superposed on Gaussian maps. It will be shown that the SMD is such a statistical variable. A similar and even more effective statistic, the MSD will be discussed in Sec. IV.

Consider a pixel array (Fig. 1) of n pixel Gaussian random variables X_j with a step function covering the whole array, superposed such that the discontinuity is located just after pixel i_0. To every pixel k of the array, we may associate the random variable Y_k defined as the difference between the mean value of the pixels 1 through k minus the mean value of the pixels $k+1$ through n. It is straightforward to show that

$$Y_k = \Delta\overline{X}_k + 2\alpha \frac{n-i_0}{n-k} \quad k \in [1, i_0] \tag{15}$$

$$Y_k = \Delta\overline{X}_k + 2\alpha \frac{i_0}{k} \quad k \in [i_0, n-1] \tag{16}$$

where $\Delta\overline{X}_k \equiv 1/k \Sigma_{j=1}^{k} X_j - 1/(n-k)\Sigma_{j=k+1}^{n} X_j$. Thus we have constructed a new array Y_k, $(k=1,\ldots,n-1)$ from the SMD of the original array. We will focus on the average value Z of the SMD defined as:

$$Z = \frac{1}{n-1} \sum_{k=1}^{n-1} Y_k . \tag{17}$$

Using Eqs. (15)–(17) we obtain

$$Z = \frac{1}{n-1}\left[\sum_{k=1}^{n-1} \Delta\overline{X}_k + 2\alpha \left(\sum_{k=1}^{i_0} \frac{1 - i_0/n}{1-k/n} + \sum_{k=i_0+1}^{n-1} \frac{i_0/n}{k/n} \right) \right]. \tag{18}$$

With the definitions $f \equiv i_0/n$, $\xi \equiv k/n$ and the assumption $n \gg 1$, we obtain:

$$Z = \frac{1}{n-1} \sum_{k=1}^{n-1} \Delta\overline{X}_k - 2\alpha[(1-f)\ln(1-f) + f \ln f]. \tag{19}$$

Thus the mean of Z over many realizations of the array is

$$\langle Z \rangle = \frac{1}{n-1} \sum_{k=1}^{n-1} \langle \Delta\overline{X}_k \rangle - 4\alpha \left[\int_0^1 df \;\; f \ln f \right] = \alpha. \tag{20}$$

The variance of Z is due both to the underlying Gaussian map and to the variation of $f = i_0/n$ (assuming α fixed). The variance due to the Gaussian background is

$$\begin{aligned} \sigma_{1,Z}^2 &= \frac{1}{(n-1)^2} \sum_{k=1}^{n-1} \left(\frac{1}{k} + \frac{1}{n-k} \right) \\ &\simeq \frac{1}{(n-1)^2} \sum_{k=1}^{n-1} \frac{1}{k/n(1-k/n)} \\ &\simeq \epsilon \int_{\epsilon}^{1-\epsilon} \frac{d\xi}{\xi(1-\xi)}, \end{aligned} \tag{21}$$

where we have replaced Σ by $n\int d\xi$, $\epsilon = O(1/n)$, $\xi = k/n$, we have assumed $n \gg 1$ and we have used the fact that the variance of the sample mean of a standardized Gaussian population with size j is $1/j$. Now from Eq. (21), we obtain

$$\sigma_{1,Z}^2 \simeq -\epsilon \ln \epsilon^2 \simeq \frac{2 \ln n}{n}. \tag{22}$$

The variance of the f-dependent part of Z is

$$\sigma_{2,Z}^2 = \langle Z_2^2 \rangle - \langle Z_2 \rangle^2 \tag{23}$$

where $Z_2 \equiv -2\alpha[(1-f)\ln(1-f) + f \ln f]$. From Eq. (20) we have $\langle Z_2 \rangle = \alpha$ and $\langle Z_2^2 \rangle$ is easily obtained as

$$\langle Z_2^2 \rangle = \int_0^1 df Z_2^2(f) \simeq \frac{4}{3}\alpha^2. \tag{24}$$

Thus

$$\sigma_Z^2 \equiv \sigma_{1,Z}^2 + \sigma_{2,Z}^2 = \frac{2 \ln n}{n} + \frac{1}{3}\alpha^2. \tag{25}$$

In order to be able to distinguish between a Gaussian+Step map and a purely Gaussian one, at the $m\sigma$ level we demand that

$$|Z_{\alpha \neq 0} - Z_{\alpha = 0}| \geqslant m\sigma_{1Z} \tag{26}$$

where we have used the variance σ_{1Z} of a given realization. This implies that the minimum value of α, α_{min} that can be detected using this test is

$$\alpha_{min} = m \left(\frac{2 \ln n}{n} \right)^{1/2} \tag{27}$$

and for $n = O(10^3)$ we obtain $\alpha_{min} \simeq 0.2m$ which for $m=1$ is about *an order of magnitude improvement* over the corresponding sensitivity of tests based on the moments skewness and kurtosis. The reason for this significant improvement is the fact that the SMD statistical variable picks up the *coherence* properties introduced by the step function on the Gaussian map. The moments on the other hand pick up only local properties of the pixels and do not amplify the long range coherence of the step-like discontinuity.

As discussed in the Introduction [see Eq. (1)] the profile of the temperature discontinuity induced by a long string does not correspond to an exact flat step function, but has a profile that drops like $\cos(\theta - \theta_0)$ where θ_0 is the angular location of the discontinuity in one dimensional data. How-

ever for the purposes of the statistics considered here, this general profile is well approximated by an effective step function with amplitude that is typically larger than half of the maximum amplitude of the real discontinuity.

Our analysis so far has assumed that the Gaussian variables X_j are independent and that the only correlation is introduced by the superposed step-function. In a realistic setup however, the underlying Gaussian map will be derived from a roughly scale invariant spectrum and thus there will be correlations among the pixels. These correlations will also be affected by the instrument noise. In addition, our analysis has been limited so far to one dimensional maps, while most CMB experiments are now obtaining two-dimensional maps. In order to take all these effects into account, we need to apply the statistics of the SMD variable onto maps constructed by Monte Carlo simulations. This is the focus of the following section.

Clearly, cosmic variance [30] does not allow any theory to make a unique prediction for any statistical variable. Thus the role of the Monte Carlo simulations will also be used to give us an estimate of the probability for each value of a given statistical variable in the context of a given model (with or without superposed temperature discontinuities).

III. MONTE-CARLO SIMULATIONS

We start by constructing an array of n Gaussian random variables X_j, $j=1,\ldots,n$ with a power spectrum $P(k)=k^{-m}$. The process by which this type of maps are constructed is standard in the literature [34], but we will briefly repeat it here for completeness and for pedagogical purposes. The values X_j associated with the pixel j are obtained as the Fourier transform of a function $g(k)$ $(k=1,\ldots,n)$ with the following properties:

For each k, the amplitude $|g(k)|$ is an independent Gaussian random variable with 0 mean and variance $P(k)=1/k^m$.

The phase θ_k of each Fourier component $g(k)$ is an independent random variable in the range $[0,2\pi]$ with uniform probability distribution $P(\theta_k)=1/2\pi$.

The Fourier components are related by complex conjugation relations needed to give a *real* variable X_j.

The discrete Fourier transform definition used is

$$X_j=\frac{1}{\sqrt{n}}\sum_{k=1}^{n} g(k)e^{2\pi i(k-1)(j-1)/n} \tag{28}$$

and the numerical programming was implemented using *Mathematica* [35]. The array X_j obtained in the way described above is then standardized to the array X_j^s, with

$$X_j^s\equiv\frac{(X_j-\mu)}{\sigma} \tag{29}$$

where μ and σ^2 are the sample mean and sample variance for the realization of the array X_j. A new array X_j' is then constructed by superposing on the array X_j^s a step function of amplitude 2α with discontinuity at a random point i_0. The array X_j' is thus obtained as

$$X_j'=X_j^s+\alpha\frac{j-i_0}{|j-i_0|},\quad j=1,\ldots,n. \tag{30}$$

Next we apply the statistics discussed in the previous section to several realizations of the arrays X_j^s and X_j' in an effort to find the most sensitive statistic that can distinguish among them. Our goal also is to find the minimum value of α that can be distinguished by that statistic at the 1σ level, thus testing the analytical results of the previous section.

We have used a lattice with 2000 pixels and a scale invariant power spectrum which for one-dimensional data is $P(k)=k^{-1}$. This a typical lattice-size for present day (and upcoming) CMB maps. For example, each one of the quad cube faces in the COBE maps has approximately 1000 pixels even though there is not complete independence among the pixels due to beam overlap. As Eq. (27) shows, the sensitivity of the SMD statistic improves as the number of pixels in a map increases. In Table I we show the results for the skewness, the kurtosis and the average SMD for the X_j arrays, with $\alpha=0$, 0.25, 0.50 and 1.0. The SMD average was obtained as in Sec. II by first constructing the array of sample mean differences and then obtaining its average value, predicted to be equal to α by the analytical study of Sec. II.

TABLE I. A comparison of the effectiveness of the statistics considered, in detecting the presence of a coherent step discontinuity with amplitude 2α relative to the standard deviation of the underlying scale invariant Gaussian map.

α	Skewness	Kurtosis	SMD Average
0.00	0.01 ± 0.11	2.97 ± 0.19	0.02 ± 0.31
0.25	0.01 ± 0.11	2.95 ± 0.20	0.25 ± 0.33
0.50	0.02 ± 0.11	2.88 ± 0.21	0.48 ± 0.38
1.00	0.03 ± 0.20	2.82 ± 0.32	0.98 ± 0.48

These statistics were applied to 50 random realizations of the array X_j^s. The mean values of the statistics considered with their 1σ standard deviations obtained over these 50 realizations are shown in the following Table I.

The analytical prediction of Sec. II for the SMD average value α is in good agreement with the results of the Monte Carlo simulations. The standard deviation of this result is not in such a good agreement with the analytical prediction because the assumption of complete independence among pixels made by the analytical treatment is not realized in the Monte Carlo simulations. There a scale invariant spectrum was considered and thus there was a non-trivial correlation among the pixels of the arrays.

A simple way to improve further the sensitivity of the SMD statistical variable is to ignore a number l of boundary pixels of the SMD array, thus constructing its average using the SMD of pixels $l+1,\ldots,n-l$. From Eq. (21), the variance of the SMD for these pixels is significantly lower than the corresponding variance of the $2l$ pixels close to the

boundaries. In addition, if the step is located within the central $n-2l$ pixels, the SMD average may be shown to be larger than α, thus further amplifying the step signature. For $l=150$ the variance of the SMD average *is reduced* by about 20%, while the SMD average is *increased* by about 20%, thus allowing the detection of steps as low as $\alpha=0.25$ at the 1σ level. The price to pay for this sensitivity improvement is the reduction of the effective pixel area where the search for steps is made.

We have also used the SMD statistical variable for non-scale invariant power spectra and found that it works better for $P(k)=k^{-m}$ with $0\leqslant m<1$ than for $m>1$. This is to be expected because large values of m imply larger correlations among pixels which in turn leads to a smaller number of effectively independent pixels and thus a larger value for the variance of the SMD average.

It is straightforward to generalize the one dimensional Monte Carlo simulations to two dimensions. In that case we use the two-dimensional discrete Fourier transform as an approximation to an expansion to spherical harmonics. This approximation is good for small area maps of the celestial sphere. We used the following definition of the two dimensional discrete Fourier transform.

$$X(i,j)=\frac{1}{n}\sum_{k_1,k_2=1}^{n} g(k_1,k_2)e^{2\pi i[(i-1)(k_1-1)+(j-1)(k_2-1)]/n} \tag{31}$$

referring to a $n\times n$ square lattice. In order to construct the background of scale invariant Gaussian fluctuations, we used $g(k_1,k_2)$ as a complex random variable. For scale invariance, the amplitude of $g(k_1,k_2)$ was obtained from a Gaussian probability distribution with 0 mean and variance

$$\sigma^2(k_1,k_2)=P(k_1,k_2)=\frac{1}{k_1^2+k_2^2}. \tag{32}$$

This scaling law in two dimensions for the power spectrum secures scale invariance because it can easily be shown that the correlation function (obtained as the Fourier transform of the power spectrum) is invariant to scale transformations of the angular variable.

The corresponding phase θ_{k_1,k_2} for the (k_1,k_2) mode was also determined randomly from a uniform probability distribution $P(\theta_{k_1,k_2})=1/2\pi$ in order to secure Gaussianity for the map $X(i,j)$.

The corresponding map with a superposed coherent step discontinuity was obtained from the standardized Gaussian map $X^s(i,j)$ as

$$X'(i,j)=X^s(i,j)+\alpha\frac{j-ai-b}{|j-ai-b|} \tag{33}$$

where

$$a=\frac{y_2-y_1}{x_2-x_1} \tag{34}$$

$$b=y_1-ax_1, \tag{35}$$

i.e., the line of step discontinuity $j=ai+b$ is determined by the two random points (x_1,y_1) and (x_2,y_2) of the map $X(i,j)$. The skewness and kurtosis of the two maps are obtained in the usual way. For example, for the standardized Gaussian map $X^s(i,j)$, we have

$$s=\frac{1}{n^2}\sum_{i,j}^{n} X^s(i,j)^3 \tag{36}$$

$$k=\frac{1}{n^2}\sum_{i,j}^{n} X^s(i,j)^4. \tag{37}$$

The main effect of the flat sky approximation used in the considered maps is that what is straight lines in our approximate flat maps would have some curvature if the spherical maps were used. However, the fact that the discontinuities are produced by straight lines is not crucial in our study. In fact, realistic string induced discontinuities are expected to have some small curvature provided that the curvature radius is approximately the horizon scale.

The SMD statistical variable is obtained by considering a set of random straight lines bisecting the map and for each line taking the difference of the sample means from the two parts of the map. A random line here is defined as a straight line that goes through two points whose coordinates are selected randomly from a uniform distribution in the coordinate range corresponding to the map. The random selection of the pair of points secures that the map is uniformly populated by lines because each point of the map has by construction equal probability to be on one of the random straight lines. For example, consider a line defined by the random points (x_1,y_1) and (x_2,y_2) of the map. The line equation is $j=ai+b$ with a, b obtained from Eqs. (34) and (35). The SMD obtained from this line is

$$\mathrm{SMD}=\left|\frac{S_1}{n_1}-\frac{S_2}{n_2}\right| \tag{38}$$

where

$$S_1=\sum_{i=1}^{n}\sum_{j=Max[(ai+b),1]}^{n} X^s(i,j) \tag{39}$$

$$S_2=\sum_{i=1}^{n}\sum_{j=1}^{Min[(ai+b),n]} X^s(i,j) \tag{40}$$

and n_1, n_2 are the corresponding numbers of terms in the sums. For a Step+Gaussian map, the index ^{s} gets replaced by $'$.

The average and variance of the SMD is obtained by averaging over a large number of random test lines (a,b) and a large number of map realizations. The results of the application of the three statistics (skewness, kurtosis and SMD average) on 30×30 scale invariant Gaussian maps for various values of step amplitudes α are shown in Table II. Uncorrelated Gaussian noise was also superposed on the signal with signal to noise ratio 2.0. The random points defining the test

TABLE II. A comparison of the effectiveness of the statistics considered in two dimensional maps. The signal to noise ratio was 2.0. Points defining the line discontinuities were excluded from the three outermost rows and columns of the maps.

α	Skewness	Kurtosis	SMD Average
0.00	0.04 ± 0.13	3.00 ± 0.20	0.01 ± 0.03
0.25	0.02 ± 0.08	2.97 ± 0.13	0.14 ± 0.09
0.50	0.05 ± 0.14	2.91 ± 0.24	0.34 ± 0.19
1.00	0.02 ± 0.24	2.95 ± 0.30	0.56 ± 0.31

lines were excluded from the outermost three rows and columns of the maps thus reducing somewhat the variance of the SMD average.

The results of Table II are in qualitative agreement with those of Table I and with the analytical results valid for the one dimensional maps. Clearly the details of the one dimensional analysis are not valid in the two dimensional case and so the agreement cannot be quantitative. The results still indicate however that the SMD statistic is significantly more sensitive compared to conventional statistics for the detection of coherent discontinuities on CMB maps. This statistic can detect coherent discontinuities with minimum amplitude $\alpha_{min}\simeq 0.5$ at the 1σ to 2σ level where α is the amplitude relative to the standard deviation of the underlying scale invariant Gaussian map.

IV. MAXIMUM SAMPLE DIFFERENCE

An alternative statistic that can be significantly more sensitive than the SMD in certain cases is the MSD. For an one dimensional set of data, the MSD statistical variable $\mathrm{Max}(r_k)$ is defined as

$$\mathrm{Max}(r_k)=\mathrm{Max}\left(\frac{Y_k}{\sigma(Y_k)}\right) \tag{41}$$

where Y_k is given by Eqs. (15), (16) and $\sigma(Y_k)$ is the standard deviation of Y_k given by

$$\sigma(Y_k)=\sqrt{\frac{1}{k}+\frac{1}{n-k}}. \tag{42}$$

The variable r_k has variance unity and mean

$$\mu(\alpha,n,k,i_0)=2\alpha\frac{(n-i_0)/(n-k)}{\sigma(Y_k)}\quad 1<k<i_0 \tag{43}$$

$$\mu(\alpha,n,k,i_0)=2\alpha\frac{i_0/k}{\sigma(Y_k)}\quad i_0<k<n-1. \tag{44}$$

For two dimensional data sets, the index $\bar{k}$ labels *partitions* by which the two dimensional pixel-surface is divided in two parts. In the Monte-Carlo simulations studied here, we have considered only map divisions represented by straight lines. It is straightforward however to generalize this to other types of divisions. In the 2d case $Y_{\bar{k}}$ is generalized to the expression given in Eq. (38). Let the set of parameters $\bar{i}_0$ describe the location and shape of the coherent discontinuity in the 2d map (in the simplest case of a straight line discontinuity $\bar{i}_0$ represents only two numbers). Let also the set of parameters $\bar{k}$ describe the location of the sample division of the 2d map. With the sample division described by $\bar{k}$ and the coherent discontinuity location described by $\bar{i}_0$, the 2d pixel-map is divided into four parts with corresponding number of pixels N_i, $i=1,\ldots,4$. This division is shown in Fig. 2 where the parts N_i are defined. For simplicity, hereafter we will omit the bar in $\bar{i}_0$ and $\bar{k}$ thus using the same notation as in the 1d case. Thus

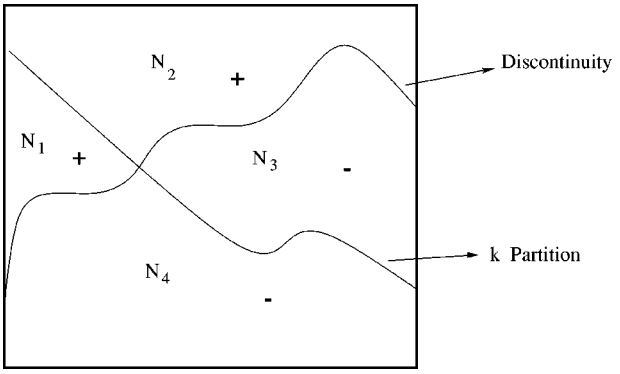

FIG. 2. The sample division described by k and the coherent discontinuity location described by i_0 divide the 2d pixel-map into four parts with corresponding number of pixels N_i, $i=1,\ldots,4$.

$$Y_k=\frac{S_1}{N_1+N_4}-\frac{S_2}{N_2+N_3} \tag{45}$$

$$\sigma(Y_k)=\sqrt{\frac{1}{N_1+N_4}+\frac{1}{N_2+N_3}} \tag{46}$$

with

$$r_k\equiv\frac{Y_k}{\sigma(Y_k)}=u_k+2\alpha\frac{w_k(i_0)}{\sigma(Y_k)} \tag{47}$$

where $u_k\equiv\Delta\bar{x}_k/\sigma(Y_k)$ is a standardized Gaussian random variable and

$$w_k(i_0)=\frac{1}{2}\left(\frac{N_1-N_4}{N_1+N_4}-\frac{N_2-N_3}{N_2+N_3}\right). \tag{48}$$

Define now $\alpha_{eff}=\alpha w_k(i_0)$. Clearly, when the partition k coincides with the discontinuity i_0 ($N_4\to 0$ and $N_2\to 0$), we have $\alpha_{eff}\to\alpha$. Otherwise, $|\alpha_{eff}|<|\alpha|$. The statistical variable r_k is Gaussian with variance unity and mean

$$\langle r_k\rangle=\frac{2\alpha_{eff}}{\sigma(Y_k)}\leqslant\frac{2\alpha}{\sigma(Y_k)}. \tag{49}$$

The $\mathrm{Max}(|r_k|)$ after n trials (partitions) is therefore a sensitive function of α_{eff} (in the limit where we take *all* possible partitions we will also have a partition with $\alpha_{eff}\to\alpha$).

Now assume that after n trials (partitions), we found $\mathrm{Max}(|r_k|)=V_0>0$. Since the variable u_k of Eq. (53) is standardized Gaussian, the probability $p_>(V_0)$ at *each trial* that we obtain a value V_0 or larger for $|r_k|$ is

$$p_>(V_0,\alpha_{eff})=\frac{1}{\sqrt{2\pi}}\int_{|V_0|}^{\infty}dr_k e^{-[r_k-(2\alpha_{eff}/\sigma(Y_k))]^2/2}+\frac{1}{\sqrt{2\pi}}\int_{-\infty}^{-|V_0|}dr_k e^{-[r_k-(2\alpha_{eff}/\sigma(Y_k))]^2/2}. \tag{50}$$

Using the binomial distribution, we find the probability for x values of r_k above V_0 after n partitions to be

$$P_x(n,V_0,\alpha_{eff})=\frac{n!}{x!(n-x)!}p_>(V_0,\alpha_{eff})^x\times(1-p_>(V_0,\alpha_{eff}))^{n-1}. \tag{51}$$

In our case we have *only one* occurrence of V_0 (since it is maximum) and the probability for this to happen is $P_1(n,V_0,\alpha_{eff})$. Thus, from a 2d pixel-map, we can measure V_0 (the maximum of r_k), n (the number of divisions used in the test) and $\sigma(Y_{k_0})$ (for the partition k_0 that corresponds to V_0). With this input, we obtain the probability distribution $P_1(\alpha_{eff})$ given n, V_0 and $\sigma(Y_{k_0})$. For example, assume that we measured V_0 with 100 divisions ($n=100$) in a 30×30 pixel map. A reasonable value of $\sigma(Y_{k_0})$ (to be obtained exactly from the data) is

$$\sigma(Y_{k_0}^-)=\sqrt{\frac{1}{N_1+N_4}+\frac{1}{N_2+N_3}}\simeq\frac{2}{\sqrt{N}}\simeq0.07. \tag{52}$$

Given n, V_0 and $\sigma(Y_{k_0})$, the probability distribution $P_1(\alpha_{eff})$ is an even function of α_{eff}, completely determined and has maxima $P_1(\alpha_{eff}^{max})$ at $\pm\alpha_{eff}^{max}$. For larger V_0 we expect larger α_{eff}^{max}.

For example, it may be easily verified using Eq. (51) and the package Mathematica that with $n=100$, we have $|\alpha_{eff}^{max}|=0$ for $V\leqslant V_0^{crit}\simeq2.5$. In general, given n, V_0 and $\sigma(Y_{k_0}^-)$, we can determine the probability distribution for α_{eff} and therefore the most probable value of α_{eff} (a lower bound on α) can be found. We also find the probability that there is no coherent discontinuity on the map as $P_1(\alpha_{eff}=0)$ (for $V_0<V_0^{crit}$ it is most probable that there is no coherent discontinuity on the map).

In Fig. 3 we show a plot of $P_1(\alpha_{eff})$ for $V_0=2.6$ (continuous line), $V_0=3.0$ (dotted line) and $V_0=4.5$ (dashed line). Notice that the probability $P_1(\alpha_{eff})$ is not normalized to unity. Instead it may be verified that $2\int_{-\infty}^{+\infty}d\alpha_{eff}P_1(\alpha_{eff})/\sigma(Y_k)\simeq0.7$ for $V_0\gtrsim2.5$, i.e., the appropriately normalized probability is $\tilde{P}_1\simeq2.8P_1/\sigma(Y_k)$. This is effectively the probability that a value V_0 will be detected as MSD given that there is a hidden discontinuity with amplitude α_{eff} in the underlying map. This can also be interpreted as the probability that there is a hidden discontinuity with amplitude α_{eff} given that a measurement has given a value V_0 for the MSD. Clearly for $V_0\leqslant2.6$, it is most probable that there is no coherent discontinuity on the map ($\alpha_{eff}^{max}=0$). On the other hand, for $V_0=3.0$, the most probable value of α_{eff} is $|\alpha_{eff}^{max}|=0.04$, while the probability that there is no coherent discontinuity on the map is about half, i.e., $P_1(\alpha_{eff}=0)\simeq P_1(\alpha_{eff}^{max})/2$.

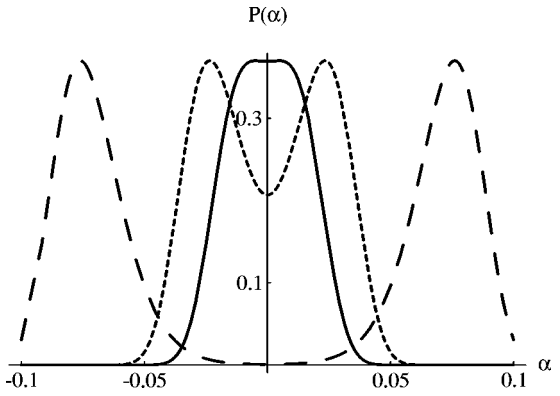

FIG. 3. A plot of $P_1(\alpha_{eff})$ for $V_0=2.6$ (continuous line), $V_0=3.0$ (dotted line) and $V_0=4.5$ (dashed line).

It is important to verify the above analytical results using Monte Carlo simulations of 2d data. We considered 2d 30×30 data sets as described in Sec. III with uncorrelated standardized Gaussian data (white noise). On these we superpose a coherent discontinuity with amplitude 2α and α in the range [0,0.45]. For each α we construct 10 maps and find V_0 and its standard deviation $\sigma(V_0)$. We also find $\sigma(Y_{k_0}^-)$ which was practically constant at $\sigma(Y_{k_0}^-)\simeq0.07$ as predicted analytically [Eq. (52)]. With the input V_0 and $\sigma(Y_{k_0}^-)$, we construct $P_1(\alpha_{eff})$ and find $|\alpha_{eff}^{max}|$, $P_1(\alpha_{eff}^{max})$ and $P_1(0)$. These results are shown in Table III.

Comparing α_{eff} with α, we confirm that in all simulated cases $|\alpha_{eff}^{max}|$ is a lower bound on $|\alpha|$. It is also clear from Table III that the MSD method can detect the presence of a coherent discontinuity with $\alpha\gtrsim0.06$ with probability ratio

$$\frac{P_1(\alpha_{eff}=0.06)}{P_1(\alpha_{eff}=0)}\simeq6. \tag{53}$$

The application of the MSD statistic discussed above was done on a white noise background with a coherent discontinuity superposed. For this type of data, we have shown that

TABLE III. The effectiveness of the MSD statistic considered in two dimensional maps with a flat spectrum of fluctuations (white noise). The first column shows the magnitude of the coherent discontinuity superposed on the standardized Gaussian map and the fourth column shows shows the *derived* most probable value value of α_{eff} (the lower bound of α) based on the MSD statistic.

α	V_0	$\sigma(Y_{\bar{k}_0})$	$\lvert\alpha_{eff}^{max}\rvert$	$P_1(0)/P_1(\lvert\alpha_{eff}^{max}\rvert)$
0.00	2.6 ± 0.5	0.07	$0.0\ \pm0.01$	1.00
0.03	2.8 ± 0.6	0.07	0.02 ± 0.02	0.83
0.06	3.4 ± 0.7	0.07	0.04 ± 0.02	0.16
0.1	4.1 ± 0.7	0.07	0.06 ± 0.03	0.01
0.2	5.6 ± 0.7	0.07	0.11 ± 0.03	0.0
0.25	7.5 ± 0.7	0.07	0.18 ± 0.03	0.0
0.3	9.0 ± 0.9	0.07	0.24 ± 0.03	0.0
0.35	9.8 ± 0.8	0.07	0.27 ± 0.03	0.0
0.4	10.4 ± 1.1	0.07	0.29 ± 0.03	0.0
0.45	12.4 ± 1.6	0.07	0.36 ± 0.04	0.0

the MSD statistic is significantly more sensitive even compared to the SMD statistic in revealing the existence of the discontinuity hidden in the data. This task however becomes more difficult if the background data are not just Gaussian white noise (or noise dominated), but are Gaussian scale invariant or have even stronger correlations (steeper spectrum). The reason is that stronger correlations tend to mimic the existence of a coherent discontinuity by the formation of large pixel clusters of higher or lower temperatures. In fact, we have shown using additional Monte-Carlo simulations of correlated data that the MSD statistic is not as robust as the SMD statistic. When we include correlations in the data (e.g., scale invariance), the sensitivity of the MSD statistic drops rapidly to the level of the SMD statistic, i.e., it can detect a coherent discontinuity with $\alpha \gtrsim 0.4$. This implies that the MSD statistic is more useful in detecting the presence of coherent discontinuities only when applied to noise dominated data.

V. CONCLUDING REMARKS

An important issue that needs to be clarified is the following: ''What are the effects of other strings giving rise to their own step discontinuity? Do they decrease the sensitivity of the suggested statistical tests?''

No attempt is made in this paper to model the fluctuations of ''other strings.'' Any such attempt (even those of simulations) is faced with the possibility of serious errors due to incorrect assumptions. Even basic features of the string scaling solution are still under serious debate. For example, there have been serious claims recently [36] that realistic field theoretical cosmological simulations of gauged string evolution would have no wiggles for long strings and no loop component. In addition, the physical processes affecting the CMB photons are not well known especially in defect based models. The issues of reionization, fluctuations present on the last scattering surface, wiggles of long strings and other effects have only been crudely modeled so far.

Instead of attempting a rough modeling of these effects, we have made a very robust and reasonable assumption: The statistics of CMB fluctuations induced by a string network on large angular scales are either Gaussian (as was the common belief so far) or ''minimally non-Gaussian'' in the sense that the only non-Gaussianity is due to a late long string. Additional types of non-Gaussianity are not excluded and they can be classified in two categories:

(1) The types that would amplify the above defined ''minimal non-Gaussianity'' and would therefore make its detection easier by using the proposed (or other) tests. In that case the proposed tests would only be able to find a lower bound on $G\mu$ which however turns out to be cosmologically quite interesting given the sensitivity of the tests for detecting the ''minimal non-Gaussianity.''

(2) The types that tend to cancel the ''minimal non-Gaussianity'' induced by a single long string. In this case the proposed test will not be a sensitive probe for string induced non-Gaussianity and more refined tests will be required for its detection.

The qualitative features of cosmic string simulations seem to indicate that ''minimal non-Gaussianity'' most probably dominates on large angular scales (there are about 10 long strings per horizon scale with typical horizon size curvature). Cosmic variance however can play a crucial role here modifying locally the expected qualitative features of the string network. The fact remains that the proposed statistical tests are particularly sensitive in detecting special types of non-Gaussianity on CMB maps which could be associated with features induced by a cosmic string network. Therefore it is worth applying them on present and upcoming CMB data.

The question that has been addressed in this paper is the following: Given the presently known values for $\delta T/T_{rms}$ from COBE on large angular scales, what is the minimum value of $G\mu$ detectable under the above stated assumption of ''minimal non-Gaussianity''? Using the SMD or MSD statistics which are specially designed to detect coherent temperature discontinuities on top of Gaussian temperature maps, we may obtain non-trivial upper or even *lower* bounds on the values of $G\mu v_s \gamma_s$ which are highly robust and independent of the details of the string evolution and the resolution of the CMB maps. Application of these statistics on the COBE data has recently been completed [32] and is presented separately.

ACKNOWLEDGMENTS

I wish to thank N. Simatos and T. Tomaras for interesting discussions and for providing helpful comments after reading the paper. This work is the result of a network supported by the European Science Foundation. The European Science Foundation acts as catalyst for the development of science by bringing together leading scientists and funding agencies to debate, plan and implement pan-European initiatives. This work was also supported by the EU grant CHRX-CT94-0621 as well as by the Greek General Secretariat of Research and Technology grant ΠΕΝΕΔ95-1759.

[1] A. Guth and S. Pi, Phys. Rev. Lett. **49**, 1110 (1982); S. Hawking, Phys. Lett. **115B**, 295 (1982); J. Bardeen, P. Steinhardt, and M. Turner, Phys. Rev. D **28**, 679 (1983); A. Starobinsky, Phys. Lett. **117B**, 175 (1982).

[2] T. W. B. Kibble, J. Phys. A **9**, 1387 (1976); A. Vilenkin, Phys. Rep. **121**, 263 (1985); A. Vilenkin and A. P. S. Shellard, *Cosmic Strings and Other Topological Defects* (Cambridge University Press, Cambridge, England, 1994); R. Brandenberger, Proceedings of the International School of Astrophysics ''D. Chalonge,'' Erice, Italy, 1992; L. Perivolaropoulos, *Trieste HEP Cosmology*, Trieste, Italy, 1994, edited by E. Gava, A. Masiero, K. S. Narain, S. Randjbar-Daemi, and Q. Shafi (World Scientific, Singapore, 1995).

[3] A. Vilenkin, Phys. Rev. D **23**, 852 (1981).

[4] N. Turok, Phys. Rev. Lett. **63**, 2625 (1989).

[5] R. R. Caldwell, R. A. Battye, and A. P. S. Shellard, Phys. Rev. D **54**, 7146 (1996).

[6] T. Vachaspati, Phys. Rev. Lett. **57**, 1655 (1986); A. Stebbins *et al.*, Astrophys. J. **322**, 1 (1987); L. Perivolaropoulos, R. Brandenberger, and A. Stebbins, Phys. Rev. D **41**, 1764 (1990); T. Vachaspati and A. Vilenkin, Phys. Rev. Lett. **67**, 1057 (1991); D. N. Vollick, Phys. Rev. D **45**, 1884 (1992); T. Hara and S. Miyoshi, Astrophys. J. **405**, 419 (1993).

[7] R. Brandenberger, N. Kaiser, E. P. S. Shellard, and N. Turok, Phys. Rev. D **36**, 335 (1987).

[8] T. Vachaspati, Phys. Rev. D **45**, 3487 (1992).

[9] T. Vachaspati, Phys. Lett. B **282**, 305 (1992); L. Perivolaropoulos and T. Vachaspati, Astrophys. J. Lett. **423**, L77 (1994).

[10] F. R. Bouchet, D. P. Bennett, and A. Stebbins, Nature (London) **335**, 410 (1988); D. Bennett, A. Stebbins, and F. Bouchet, Astrophys. J. Lett. **399**, L5 (1992); B. Allen, R. R. Caldwell, S. Dodelson, L. Knox, E. P. S. Shellard, and A. Stebbins, Phys. Rev. Lett. **79**, 2624 (1997).

[11] J. Gott *et al.*, Astrophys. J. **352**, 1 (1990); L. Perivolaropoulos, Phys. Rev. D **48**, 1530 (1993); R. Moessner, L. Perivolaropoulos, and R. Brandenberger, Astrophys. J. **425**, 365 (1994); J. Magueijo, Phys. Rev. D **52**, 4361 (1995); X. Luo, *ibid.* **49**, 3810 (1994); D. Coulson, P. Ferreira, P. Graham, and N. Turok, Nature (London) **368**, 27 (1994).

[12] G. Smoot *et al.*, Astrophys. J. Lett. **396**, L1 (1992); E. L. Wright *et al.*, *ibid.* **396**, L5 (1992).

[13] A. Kogut, A. J. Banday, C. L. Bennett, K. M. Gorski, G. Hinshaw, G. F. Smoot, and E. L. Wright, Astrophys. J. Lett. **464**, L29 (1996); A. Kogut, A. J. Banday, C. L. Bennett, G. Hinshaw, P. M. Lubin, and G. F. Smoot, *ibid.* **439**, L29 (1995); G. Hinshaw, A. J. Banday, C. L. Bennett, K. M. Gorski, and A. Kogut, *ibid.* **446**, L67 (1995); G. Hinshaw, A. Kogut, K. M. Gorski, A. J. Banday, C. L. Bennett, C. Lineweaver, C. Lubin, G. F. Smoot, and E. L. Wright, *ibid.* **431**, 1 (1994); G. F. Smoot, L. Tenorio, A. J. Banday, A. Kogut, E. L. Wright, G. Hinshaw, and C. L. Bennett, *ibid.* **437**, 1 (1994).

[14] P. G. Ferreira, J. Magueijo, and K. M. Gorski, ''Evidence for non-Gaussianity in the DMR Four Year Sky Maps,'' astro-ph/9803256, 1998.

[15] A. Lewin, A. Albrecht, and J. Magueijo, ''A new statistic for picking out Non-Gaussianity in the CMB,'' astro-ph/9804283, 1998; P. G. Ferreira and J. Magueijo, Phys. Rev. D **56**, 4578 (1997); **56**, 4578 (1997); **55**, 3358 (1997).

[16] J. Robinson and A. Albrecht, Mon. Not. R. Astron. Soc. **283**, 733 (1996).

[17] A. Albrecht, R. Battye, and J. Robinson, Phys. Rev. Lett. **79**, 4736 (1997).

[18] B. Allen, R. Caldwell, E. P. S. Shellard, A. Stebbins, and S. Veeraraghavan, Phys. Rev. Lett. **77**, 3061 (1996).

[19] G. F. Smoot, ''The CMB Anisotropy Experiments,'' astro-ph/9705135, 1997.

[20] D. Scott, J. Silk, and M. White, Science **268**, 829 (1995); PLANCK 1998, Homepage: http://astro.estec.esa.nl/SA-general/Projects/Planck/planck.html; MAP 1998, Homepage: http://map.gsfc.nasa.gov

[21] S. Veeraraghavan and A. Stebbins, Astrophys. J. **365**, 37 (1990); A. Stebbins, *ibid.* **327**, 584 (1988); R. Brandenberger and N. Turok, Phys. Rev. D **33**, 2182 (1986); L. Perivolaropoulos, Phys. Lett. B **298**, 305 (1993).

[22] N. Kaiser and A. Stebbins, Nature (London) **310**, 391 (1984); R. Gott, Astrophys. J. **288**, 422 (1985).

[23] D. Bennett and F. Bouchet, Phys. Rev. Lett. **60**, 257 (1988); A. Albrecht and A. Stebbins, *ibid.* **69**, 2615 (1993); B. Allen and A. P. S. Shellard, *ibid.* **64**, 119 (1990).

[24] L. Perivolaropoulos, Astrophys. J. **451**, 429 (1995).

[25] L. Perivolaropoulos, Mon. Not. R. Astron. Soc. **267**, 529 (1993).

[26] A. Gangui, Phys. Rev. D **54**, 4750 (1996); J. Magueijo, *ibid.* **52**, 689 (1995).

[27] P. Graham, N. Turok, P. M. Lubin, and J. A. Schuster, Astrophys. J. **449**, 404 (1995).

[28] M. P. Pompilio, F. R. Bouchet, G. Murante, and A. Provenzale, Astrophys. J. **449**, 1 (1995).

[29] R. Scaramella and N. Vittorio, Astrophys. J. **375**, 439 (1991).

[30] M. Srednicki, Astrophys. J. Lett. **416**, L1 (1993).

[31] A. Gangui, F. Lucchin, S. Matarrese, and S. Mollerach, Astrophys. J. **430**, 447 (1994).

[32] L. Perivolaropoulos and N. Simatos, astro-ph/9803321, 1998.

[33] R. E. Walpole, R. H. Myers, and S. Myers, Probability and Statistics for Engineers and Scientists (Prentice Hall, Englewood Cliffs, NJ, 1998).

[34] J. R. Bond and G. Efstathiou, Mon. Not. R. Astron. Soc. **226**, 665 (1987).

[35] S. Wolfram, *Mathematica version 3.0* (Addison-Wesley, Reading, MA, 1996).

[36] G. Vincent, M. Hindmarsh, and M. Sakelariadou, Phys. Rev. D **56**, 637 (1997).